Density-Transition Scale at Quasiperpendicular Collisionless Shocks

S. D. Bale* and F. S. Mozer
Space Sciences Laboratory and Department of Physics, University of California, Berkeley, California 94720, USA
T. S. Horbury
The Blackett Laboratory, Imperial College, London SW7 2BW, United Kingdom
(Received 23 May 2003; published 31 December 2003)

Measurements of a spacecraft floating potential, on the four Cluster spacecraft, are used as a proxy for electron plasma density to study, for the first time, the macroscopic density transition scale at 98 crossings of the quasiperpendicular terrestrial bow shock. A timing analysis gives shock speeds and normals; the shock speed is used to convert the temporal measurement to a spatial one. A hyperbolic tangent function is fitted to each density transition, which captures the main shock transition, but not overshoot or undershoot nor foot features. We find that, at a low Mach number M, the density transition is consistent with both ion inertial scales c/ω_{pi} and convected gyroradii $v_{sh,n}/\Omega_{ci,2}$, while at $M \geq 4$–5 only the convected gyroradius is the preferred scale for the shock density transition and takes the value $L \approx 0.4 v_{sh,n}/\Omega_{ci,2}$.

DOI: 10.1103/PhysRevLett.91.265004 PACS numbers: 52.35.Tc, 96.50.Fm

Collisionless shocks in plasmas heat and compress an incoming flow over spatial scales much smaller than a collisional mean free path. The terrestrial bow shock forms from a fast-model magnetohydrodynamics wave once nonlinear steepening from the $(\vec{u}\cdot\vec{\nabla})\vec{u}$ term in the equation of motion is balanced by some dispersive of dissipative process, whose role is to transport away or damp out high frequency components of the nonlinearity. From the two-fluid point of view, the relevant spatial scales are the electron and ion inertial lengths c/ω_{pe} and c/ω_{pi} associated with dispersion, the magnetic Reynolds length $R_m \approx \eta/(\mu_0 v_{sh})$ associated with some anomalous resistivity η, and the kinetic Reynolds length $R_e \approx \mu/(\rho v_{sh})$ for some viscosity μ, where v_{sh} is the shock velocity in the plasma frame. Thermal conduction does not effectively dissipate energy in collisionless shocks. The final transition scale of the shock is determined by the largest of these scales encountered during steepening that balances the nonlinearity.

Up to some "critical" Mach number ($M_c \approx 2.67$ for $\beta = 0$), dispersion and/or resistivity can support the shock structure [1] and the steady-state shock transition scale will be the larger of the dispersive (c/ω_{pi}) or resistive (R_m) scales. Magnetic transition scales of $\approx c/\omega_{pi}$ have been observed, using two-point measurements, at various subcritical shocks [2–4]. At higher Mach numbers, a viscous force is needed to balance the nonlinearity [5]. In the fluid scenario, this can be thought of as the result of a gyroviscosity associated with gradients of the ion stress tensor. The analytical form of this viscous term in an inhomogeneous field is not known, though its scale size is assumed to be the gyroscale of trapped ions in the shock front.

Astrophysical and heliospheric shocks are also abundant sources of energetic particles and the proposed acceleration mechanisms, which are not fully understood, seem to depend on the spatial scales of the shock [6–8]. This can be seen by solving the electron and ion equations of motion, giving the "generalized Ohm's law" [9] for the electric field, which is the source of energization,

$$\vec{E} + \vec{v}\times\vec{B} \approx \frac{\vec{j}\times\vec{B}}{ne} - \frac{\vec{\nabla}\cdot\overleftrightarrow{P}_e}{ne} - \frac{m_e}{M_i}\frac{\vec{\nabla}\cdot\overleftrightarrow{P}_i}{ne} + \eta\vec{j} + \frac{m_e}{ne^2}\frac{d\vec{j}}{dt}. \quad (1)$$

The terms on the right side of Eq. (1) become important on different scales [10]; hence the stationary electric field scale depends on the balance of the dispersive ($\vec{j}\times\vec{B}$), ambipolar ($\vec{\nabla}\cdot\overleftrightarrow{P}_e$), viscous ($\vec{\nabla}\cdot\overleftrightarrow{P}_i$), resistive ($\eta\vec{j}$), and nonlinear ($d\vec{j}/dt$) physics.

While the magnetic structure of collisionless shocks is fairly well documented, measurements of the density transition scale of shocks are rare, if not absent in the literature. This is primarily because particle counting instruments traditionally have required one spacecraft spin to acquire a complete distribution function measurement and spacecraft spin rates are on the order of seconds. In this Letter we present the first study of the density transition scale at 98 collisionless shocks and show that the natural scale of the transition is the convected ion gyroradius $v_{sh,n}/\Omega_{ci,2}$, where $v_{sh,n}$ is the shock speed in the plasma frame and $\Omega_{ci,2}$ is the downstream ion gyrofrequency. This is in contrast with previous work on magnetic transition scales [2,3], which suggests the ion inertial scale, for a smaller range of (low) Mach numbers.

The Electric Field and Waves experiment on Cluster II [11] is a double probe dc electric field experiment that measures probe-to-probe and probe-to-spacecraft electric potentials. The probe-to-probe measurement is a measure

of the local electric field in the plasma, while the probe-to-spacecraft measurement is the floating potential of the spacecraft with respect to the plasma. A sunlit spacecraft in a plasma emits a spectrum of photoelectrons with a typical e-folding energy of 1 eV; in a low density plasma, the spacecraft charges positive and draws a return (electron) current from the plasma. Hence, the equilibrium floating potential of the satellite is related to ambient density of the plasma by some function [12,13]. Here we use the function $n[\phi(t)] = \sum_{i=1}^{3} a_i 10^{b_i \phi(t)}$ (hereafter "density proxy"), where ϕ is the average of the measured probe-to-spacecraft potential on four spin-plane probes and the coefficients have been determined by fitting to measured plasma density using a particle counting experiment on the Cluster spacecraft; in the relatively dense solar wind/magnetosheath, one term of the sum dominates. This technique is described in the literature [12,13]. Spacecraft potential, hence $n(\phi)$, is sampled 5 times/sec on each spacecraft, compared to one measurement each 2–4 sec for the electron and ion particle counting instruments. Use of $n(\phi)$ allows a full sampling of the shock density transition, which occurs on time scales of 1–10 sec. We also use averages of magnetic field vectors from the fluxgate magnetometer instruments [14], in the asymptotic upstream and downstream states. The solar wind velocity and alpha/proton ratio are measured at the Advanced Composition Explorer (ACE) spacecraft, at the L1 libration point, and translated back to earth by the solar wind travel time. These data compare well with locally sampled solar wind data from Cluster and allow us to study shocks from early in the mission when the Cluster solar wind instruments were not yet operative. Small differences in the contact potential between the electric field probes (8 cm spheres) and the plasma, as well as shadowing during spacecraft rotation, produce a narrow band tone in the data at harmonics of the spacecraft spin frequency $f_{sc} \approx 1/4$ Hz. We apply a narrow digital notch filter at f_{sc}, $2f_{sc}$, and $4f_{sc}$ to $\phi(t)$ to remove this effect. Between 22 December 2000 and 28 May 2001, Cluster encountered the quasiperpendicular bow shock more than 100 times. Here we analyze 98 shock crossings, where fits to $n(\phi)$ are possible and ACE solar wind data exist. Data from the four spacecraft are used to find the shock normal vector $\hat{n}$ and speed along in the normal u_n. An example is shown in Fig. 1 from a shock encountered at 01:26 on 25 December 2000. The four spacecraft measurements of smoothed spacecraft floating potential are shown as different colors. The time derivative of the spacecraft potential measurement is cross correlated between spacecraft pairs (1-2, 1-3, 1-4) as a function of a time lag Δt. The peak of the cross-correlation function corresponds to the optimal time lag τ_{ij} between spacecraft i and j. Often the best time lag is found by the eye, as turbulence in the density data produces several lags with similar correlation coefficients. Then, the shock normal $\hat{n}$ and speed u_n (in the spacecraft frame) are calculated by

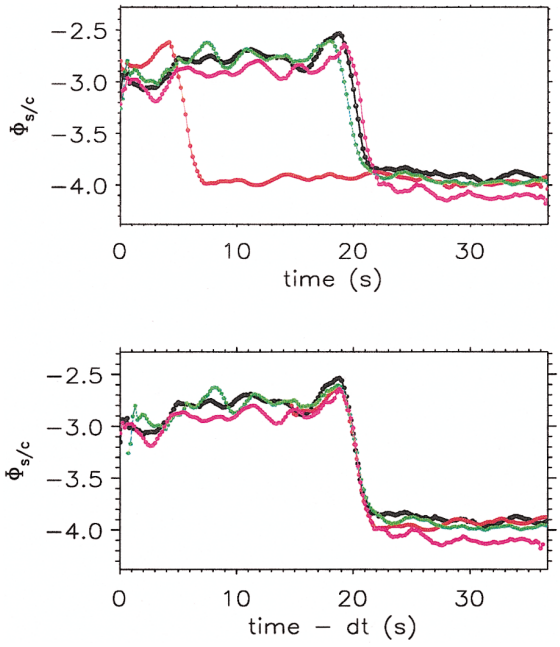

FIG. 1 (color). Smoothed spacecraft potential measurements $-\phi_{sc}$ from the four Cluster spacecraft (each as a different color) at a collisionless shock. The time shift between encounters on the four spacecraft is used to compute the shock normal vector and speed. Notice also the coherence of the first cycle of the overshoot.

solving the matrix equation $\overleftrightarrow{r} \cdot \hat{n} = u_n \vec{\tau}$, where τ is the vector of time lags ($\tau_{12}, \tau_{13}, \tau_{14}$) and $\overleftrightarrow{r}$ is the matrix of spacecraft separation vectors. This technique assumes that the shock is locally planar and moves at constant normal velocity, which is true to first order. It can be seen in Fig. 1 that the shock ramp and overshoot structure are spatially coherent on the scale of spacecraft separation, which ranges from 600 to 1100 km for this example.

Figure 2 shows the histogram of the magnetosonic Mach number for these shocks, defined as $M_{ms} = |v_{sh,n}|/c_{ms}$, where $c_{ms} = (c_s^2 + v_A^2)^{1/2}$ is the magnetosonic

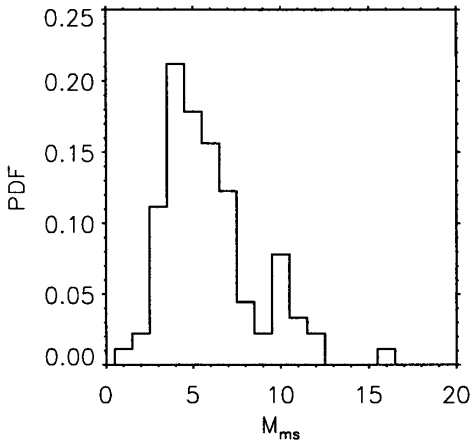

FIG. 2. Probability distribution of the magnetosonic Mach number for 98 quasiperpendicular shocks.

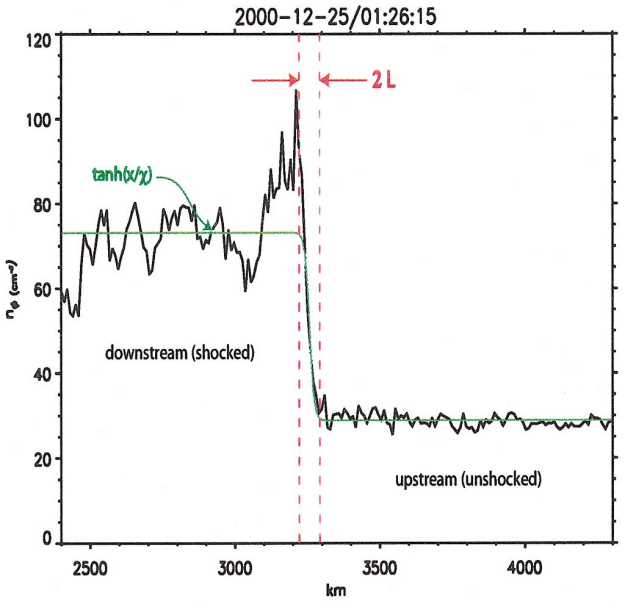

FIG. 3 (color). Density transition from downstream (shocked) to upstream (unshocked) states for a Mach $M_{ms} \approx 3.5$, $\Theta_{Bn} \approx 81°$ shock. The green line is the hyperbolic tangent fit; red vertical lines show the density transition scale.

speed, c_s is the sound speed, and v_A is the Alfvén speed. $v_{sh,n}$ is the shock normal velocity in the plasma frame, which is calculated as $\vec{v}_{sh,n} = u_n\hat{n} - \vec{v}_{sw}$ and $\vec{v}_{sw}$ is the solar wind velocity in the spacecraft frame. The Alfvén speed is computed using the measured alpha/proton ratio. Mach numbers around $M_{ms} \approx 4$ are most common in our data set, indicating primarily supercritical shocks. The magnetic field contact angle Θ_{Bn}(not shown) has a broad distribution between 43° and 90°; all of the shocks are quasiperpendicular (by choice). The time series $n[\phi(t)]$ becomes a spatial measurement with $\Delta x = u_n t$. In Fig. 3, the density transition from the dense magnetosheath, through the shock, into the solar wind is shown for the Mach $M_{ms} \approx 3.5$, $\Theta_{Bn} \approx 81°$ shock in Fig. 1. A hyperbolic tangent function (green line) $n(x) = n_0 + n_1 \tanh(x/\chi)$ is fitted to the density proxy data and the macroscopic density transition scale is then defined to be $L = n(0)/|dn(0)/dx| = \chi n_0/n_1$; vertical dotted lines show $\pm L$, confirming that L is a good measure of shock thickness. Overshoot/undershoot structure is not measured with this technique, nor is shock pedestal (foot) structure. The coefficients from the fit can be expressed as $n_0 = (n_d + n_u)/2$ and $n_1 = (n_d - n_u)/2$, where n_u is the upstream (unshocked) plasma density and n_d is the downstream (shocked) density; therefore, the scale length $L = (n_d + n_u)/(n_d - n_u)\chi$. If the true density is different from the proxy by a multiplicative constant, it will cancel and L is unaffected. If the true density differs by an additive constant n', then the new (true) scale length is $L' = L[1 + 2n'/(n_d + n_u)]$. Comparing our spacecraft potential density proxy $n(\phi)$ with the ACE density

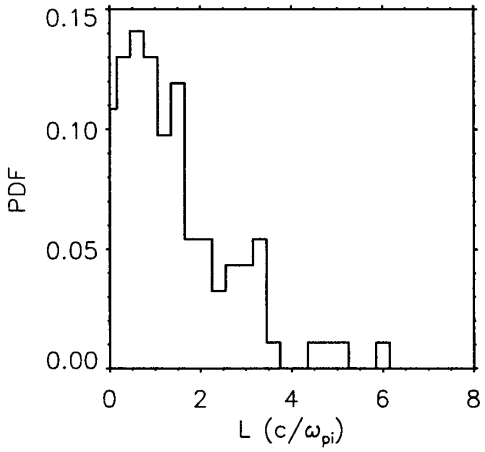

FIG. 4. Distribution of shock scale size L in units of ion inertial lengths c/ω_{pi}. The distribution is broadly peaked near $0.5c/\omega_{pi}$.

data, we estimate $n'/n_u \approx 5\%$, which becomes the error on our length scale measurement L. This measure of shock thickness, for the 98 shocks, gives a broad distribution of scales from a few km to 400 km, consistent with previous two-point measurements [2,15].

Generally, shocks show some substructure within the ramp, some of which is coherent and clearly spatial and others a more turbulent structure. Our technique does not capture the scales associated with this turbulence, rather only the largest transition scale at the shock. Figure 4 shows the probability distribution of shock density scales L normalized to the upstream ion inertial length c/ω_{pi}, which is peaked at near $0.5c/\omega_{pi}$(in bins of $0.3c/\omega_{pi}$). The ion inertial scale is associated with the introduction of Hall current terms in a generalized Ohm's law and indicates the demagnetization of solar wind ions in the current layer of the shock; it is the fundamental scale of

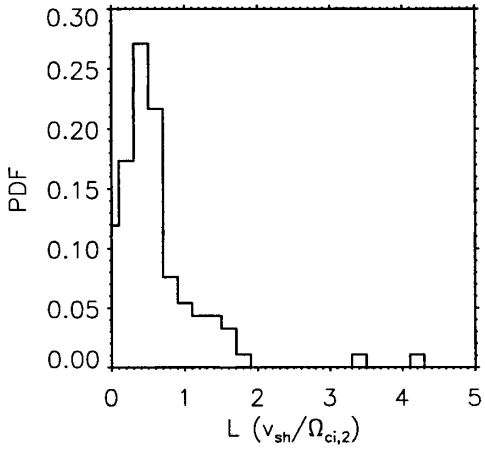

FIG. 5. Distribution of shock scale size L in units of convected ion gyroradii $v_{sh,n}/\Omega_{ci,2}$. This distribution shows a sharp peak at near $0.4v_{sh,n}/\Omega_{ci,2}$, indicating a good measure of the shock scale.

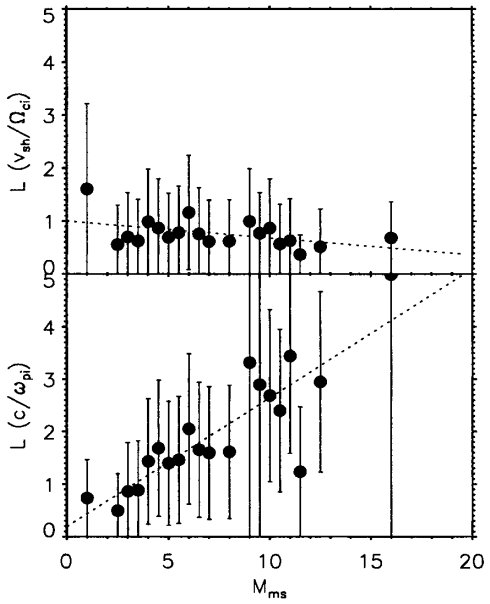

FIG. 6. Relationship between scale size and the magnetosonic Mach number. $L/(v_{sh,n}/\Omega_{ci,2})$ (upper panel) is approximately constant over a large range of Mach number, while the ion inertial scaling (lower panel) increases with Mach number.

the dispersion that has been suggested to balance steepening at low Mach numbers [1]. In Fig. 5, the density scale L is normalized to the convected ion gyroradius $v_{sh,n}/\Omega_{ci,2}$, where $v_{sh,n}$ is the shock normal velocity in the solar wind frame, and $\Omega_{ci,2}$ is the downstream proton gyrofrequency; $v_{sh,n}/\Omega_{ci,2}$ is a measure of the gyroradius of solar wind protons that gyrate, and may be trapped, around the shock ramp. The sharp peak in the histogram at $L \approx 0.4 v_{sh,n}/\Omega_{ci,2}$ suggests that the convected gyroradius is an appropriate measure of shock thickness over our range of Mach numbers.

The dependence on the magnetosonic Mach number is shown in Fig. 6. Data are averaged into bins of $0.5M_{ms}$, error bars are 1 standard variation of the length scale within the bin, or the length scale itself for bins containing one measurement. The convected ion gyroradius $v_{sh,n}/\Omega_{ci,2}$(upper panel) appears to be the preferred scale to describe the shock density transition over the range of Mach numbers 1–15, with some dispersion at the low end of the scale. The ion inertial scale c/ω_{pi} (lower panel) is appropriate at small Mach numbers only. It should be noted that $(v_{sh,n}/\Omega_{ci,2})/(c/\omega_{pi}) \propto M$; if the natural transition scale of the shock is $v_{sh,n}/\Omega_{ci,2}$, then $L/(c/\omega_{pi})$ (lower panel) should scale as M, which it appears to do.

In summary, we show that the convected ion gyroscale $v_{sh,n}/\Omega_{ci,2}$ is the natural scale of the quasiperpendicular collisionless shock density transition scale from Mach numbers of $M \gtrsim 4$ into the supercritical range; the preferred scale is $L \approx 0.4 v_{sh,n}/\Omega_{ci,2}$. At the lowest Mach numbers, both the ion inertial scale c/ω_{pi} and the gyroscale are comparable and are good measures of thickness. The velocity transition scale should be identical, as conservation of mass requires $n\ v = \text{const}$ in the shock frame. It is possible that the magnetic ramp has a different scale, if the dispersive or resistive scale lengths are larger than the viscous length R_e [5,16]. However, this seems unlikely as large Mach number shocks have scales of several dispersive scales c/ω_{pi}.

Work at the University of California, Berkeley is supported by NASA Grants No. NAG5-11944 and No. NAG5-12483. T. H. is supported by PPARC (U.K.).

*Electronic address: bale@ssl.berkeley.edu

[1] W. Marshall, Proc. R. Soc. London A **233**, 367 (1955).
[2] C. T. Russell *et al.*, Geophys. Res. Lett. **9**, 1171 (1982).
[3] M. M. Mellott and W. A. Livesey, J. Geophys. Res. **92**, 13 661 (1987).
[4] M. Balikhin *et al.*, Adv. Space Res. **15**, 247 (1995).
[5] F. Coroniti, J. Plasma Phys. **4**, 265 (1970).
[6] M. A. Lee, V. D. Shapiro, and R. Z. Sagdeev, Geophys. Res. Lett. **101**, 4777 (1996).
[7] M. Scholer *et al.*, J. Geophys. Res. **108**, 1014 (2003).
[8] M. Hoshino and N. Shimada, Astrophys. J. **572**, 880 (2002).
[9] B. Rossi and S. Olbert, *Introduction to the Physics of Space* (McGraw-Hill, New York, 1970).
[10] V. M. Vasyliunas, Rev. Geophys. Space Phys. **13**, 303 (1975).
[11] G. Gustafsson *et al.*, Space Sci. Rev. **79**, 137 (1997).
[12] A. Pedersen, Ann. Geophys. **13**, 118 (1995).
[13] A. Pedersen *et al.*, Ann. Geophys. **19**, 1483 (2001).
[14] A. Balogh *et al.*, Ann. Geophys. **19**, 1207 (2001).
[15] J. D. Scudder *et al.*, J. Geophys. Res. **91**, 11 053 (1986).
[16] C. F. Kennel, J. Geophys. Res. **93**, 8545 (1988).